Summer 8-1-2024

Variability in Nutrient Concentrations Across Regions of the Winyah Bay River Plume

Anne Mackenzie Gossman
Coastal Carolina University

Variability in Nutrient Concentrations Across Regions of the Winyah Bay River Plume

by

Anne Mackenzie Gossman

A Thesis submitted
in Partial Fulfillment of the Requirements for the
Degree of Master of Science in
Coastal Marine and Wetland Studies

Gupta College of Science

Coastal Carolina University

2024

Dr. Diane Bennett Fribance
_____
Graduate Faculty Advisor, Coastal Carolina Univ.

Dr. Angelos Hannides
_____
Committee Member, Coastal Carolina Univ.

Dr. Lindsey Bell
_____
Committee Member, Coastal Carolina Univ.

Dr. Alexander Yankovsky
_____
Committee Member, Univ. of South Carolina

Dr. Zhixiong Shen
_____
MSCI Associate Chair of Graduate Programs

Dr. Chad Leverette
_____
Dean, Gupta College of Science

This work is dedicated to my fiancé Miles. Thank you for your constant support and all you have done for me. I will forever be grateful.

Acknowledgments

This material is based upon work supported by the U.S. National Science Foundation under Grant Nos. OCE-2148479 and OCE-2148480

Thank you to the Coastal Carolina University Department of Marine Science Coastal and College of Graduate and Continuing Studies.

Special thanks to the crews of the *R/V Savannah* and *R/V Coastal Explorer*, my colleagues in the physical oceanography laboratory and at the University of South Carolina, and most of all my advisor Dr. Fribance and committee members Dr. Hannides, Dr. Bell, and Dr. Yankovsky.

Abstract

River plumes are one of the few large-scale features responsible for transporting particulates and terrigenous materials to coastal oceans. Macro-nutrients, such as dissolved inorganic nitrogen (DIN) and phosphorus (PO_4^{3-}), are basic requirements for marine food webs. Due to the plumes' ability to transport large quantities of these constituents, these systems contribute heavily to coastal productivity. This study focuses on the dynamics of the Winyah Bay river plume located in Georgetown, South Carolina. River plumes, including the Winyah Bay plume, are dynamic systems whose structures are comprised of a multitude of regions and features including the source, lift off, near-field, mid-field, and far-field regions, and plume fronts. Prior studies have focused on the physical dynamics of the Winyah Bay plume regions and features but have not yet examined the nutrient dynamics of this system. The objective of this study was to evaluate the distribution of DIN and phosphate through the different regions of the Winyah Bay plume. Four characteristics (salinity, temperature, plume depth, and Froude number) were used to characterize plume regions using multiple linear regression, and no correlations between the nutrient concentrations and the plume region characteristics were identified. The limited size of the data set may have contributed to the lack of statistical significance. At the plume fronts, however, there was significant accumulation of nutrients on the estuarine side indicating these are important structures contributing to coastal productivity. Despite the limitations of a small sample size and intensive sampling techniques, this study provides a starting point for future research into the nutrient dynamics of the Winyah Bay river plume and its impact on coastal productivity.

Table of Contents

List of Tables

List of Figures

List of Symbols, Acronyms and Abbreviations

Symbol/Acronym/ Abbreviation	Definition
ADCP	Acoustic Doppler Current Profiler
Ave	Average
CTD	Conductivity, Temperature, Depth
D	Plume Depth
DIN	Total Dissolved Inorganic Nitrogen
Fr	Froude Number
g'	Reduced Gravity
h	Total water depth
H1	Hypothesis 1
H2	Hypothesis 2
N	Nitrogen
NH_4^+	Ammonium
NO_2^-	Nitrite
NO_3^-	Nitrate
P	Phosphorus
PO_4^{3-}	Phosphate
SAB	South Atlantic Bight
SD	Standard Deviation
TKE	Total Kinetic Dissipation
u	East/West velocity component
v	North/South velocity component

V	Velocity Magnitude
VMP	Vertical Microstructure Profiler
WBP	Winyah Bay Plume

1. Introduction

Rivers play a critical role as conduits for transporting essential nutrients like nitrogen (N) and phosphorus (P) to coastal oceans (Sharples et al., 2017). These nutrients are vital for primary productivity, thereby significantly contributing to the biological productivity of coastal ecosystems (Giraud et al., 2008). Thus, understanding river plumes, which are complex systems composed of multiple dynamic regions influenced by various environmental forcings (Horner-Devine et al., 2015), is crucial. This study aims to observe and enhance our understanding of how N and P behave and are distributed within these plume regions, advancing our knowledge of nutrient dynamics in coastal environments.

1.1. Nutrients

Nutrients can be grouped into two categories, macro and micro-nutrients. While micro-nutrients have been known to limit primary production, macro-nutrients are defined as the nutrients required in large quantities for productivity to take place. Macro-nutrients such as dissolved inorganic N (DIN) and P are basic requirements for biological productivity and thus support our local fisheries and economies (Gomes et al., 2018a). DIN is found in the forms of nitrate (NO_3^-), nitrite (NO_2^-), and ammonium (NH_4^+) with NO_3^- being the predominant useable form of DIN in the oceans (Voss et al., 2013). This NO_3^- can be assimilated after sequential reduction to NO_2^- and NH_4^+ (Zehr & Ward, 2002). NO_3^- can be supplied through mixing, advection and diffusion from deep water, atmospheric deposition, and through terrestrial runoff (Zehr & Ward, 2002). According to Voss et al. (2013) roughly 40-66 Tg of N is transported to coastal oceans through rivers each year with

40% occurring as DIN. P, however, cannot be fixed by the atmosphere and is predominantly transported to the oceans via riverine influx (Paytan & McLaughlin, 2007). Phosphate (PO_4^{3-}), the predominant form of inorganic P, is assimilated by phytoplankton into organic P which is then transferred to higher trophic levels when the phytoplankton are ingested (Paytan & McLaughlin, 2007). This organic P is then transformed back into PO_4^{3-} through the fecal material or decomposition of these organisms (Paytan & McLaughlin, 2007). While both N and P are vital to life, and each possess the ability to limit primary production, in some coastal regions the supply of these nutrients can exceed the demand set by primary producers.

Over the last several hundred years the total inputs of N and P into coastal oceans has roughly doubled (Beusen et al., 2012; Jickells et al., 2017; Seitzinger et al., 2010). Anthropogenic activities have greatly increased the levels of N and P in coastal environments causing various environmental issues (Galloway et al., 2008) including eutrophication, hypoxia, and acidification events (Cai et al., 2011; Lam & Kuypers, 2011; Seitzinger & Phillips, 2017). Several studies have found that such increases in nutrient loads negatively affect water quality and biodiversity in coastal areas (Bouwman et al., 2005). He et al. (2023) found that increases to N and P concentrations resulted in a higher eutrophication index. These results coupled with those of Cloern, (2001), who found that the use of fertilizers has increased fluvial nitrogen loading to coastal oceans, suggest the importance in understanding nutrient distributions through riverine outflows.

1.2 River Plumes

River plumes, classified as outflows of buoyant freshwater that mix with ambient coastal waters (Horner-Devine et al., 2015), are one of the few large-scale features

responsible for transporting nutrients and terrigenous particulates to coastal oceans (Trenberth et al., 2007). These plumes are ever-changing dynamic systems that are greatly affected by a variety of conditions. The size and shape of these structures are influenced by freshwater discharge, tidal amplitude, coastline bathymetry, ambient ocean currents, wind stress, and Earth's rotation (Horner-Devine et al., 2015). It is the combination of these conditions that determine plume scale and structure; however, freshwater discharge has the greatest variability and thus heavily influences the plume's persistence through tidal cycles (Horner-Devine et al., 2015). Plumes with small discharges tend to dissipate and form anew with each tidal cycle whereas plumes with large discharges tend to persist through multiple tidal periods (Horner-Devine et al., 2015).

1.2.1 Regions of a plume

River plumes are comprised of various dynamic regions that are not consistently defined in the literature (Cole & Hetland, 2016). A variety of parameters have been developed to assist in the characterization of these zones; however, these parameters cannot be used independently to define these areas. A combination of multiple parameters and measurements are required to distinguish between these regions. The primary objective of this study is to explore how the concentrations of DIN and PO_4^{3-} change through the different regions of a plume system. For the purposes of this study, I will be using definitions of plume regions provided by Horner-Devine et al. (2015) which are as follows:

1. The source region is the location at which the initial buoyancy and momentum are set.
2. The liftoff zone, where the buoyant freshwater layer loses contact with the bottom. This region is also the location where the plume becomes supercritical with an upper layer Froude number (F_r) equal to 1, further described in section 2.3.3.

3. The near-field region begins at the liftoff zone and is the location where momentum exceeds the buoyancy-driven velocity (or gravity current propagation speed) of the plume layer (F_r >1).
4. The mid-field region is a transitional zone from the momentum dominated near-field to the wind or geostrophic dominated far field. This region can sometimes contain a bulge where a fraction of the freshwater discharge is entrained in an anticyclonic eddy before exiting in the downstream propagation.
5. This is followed by the far-field region of the plume where flow is governed by Earth's rotation, wind stress, and buoyancy and is thus considered subcritical (F_r < 1).

   Horner-Devine et al. (2015) classified a prototypical plume (Figure 1a) as a structure containing all the aforementioned features.

Fronts, defined as structures usually located on the plume boundaries and distinguished by sharp gradients in fluid density (Horner-Devine et al., 2015), are important components of these systems. The velocities in plume fronts, a combination of Ekman velocity and frontal geostrophic current, are higher than in the main body of the plume (Kilcher & Nash, 2010). Thus, the Froude number could potentially be used to locate frontal structures. There are two kinds of fronts, exterior fronts are structures created from the convergence of fresh water with ambient coastal waters, whereas interior fronts are boundaries created from the convergence of a newer fresher plume with an older, higher salinity plume. This convergence leads to accumulation of materials, including nutrients, at these structures (Li et al., 2022). The accumulation of these nutrients has the potential to increase productivity at the fronts, making them regions of particular interest for further study.

1.2.2 The Winyah Bay Plume

The Winyah Bay plume (WBP), the focus of this study, has been observed to form a modification of a prototypical plume known as a "cross-shelf" plume, shown in Figure 1b (Yankovsky et al., 2022). This result is achieved when the WBP has sufficient discharge to generate supercritical flow and is forced by a combination of inertia, geostrophic transport, and Ekman transport. Thus, upwelling favorable winds are required to achieve this result. However, if the winds are too strong the plume will erode. This system, when acted upon by upwelling favorable wind conditions on a timescale of several hours to days, will divert from its typical downstream propagation, turn upstream, and cross the shelf at an oblique angle, thus earning the denotation of "cross-shelf" plume (Yankovsky et al., 2022). This cross-shelf nature allows the plume to maintain a high length to width aspect ratio, allowing the freshwater influence to reach farther across the shelf (Yankovsky et al., 2022), thus providing a potential vector for nutrient delivery farther offshore compared to when an along-coast far field transport is generated.

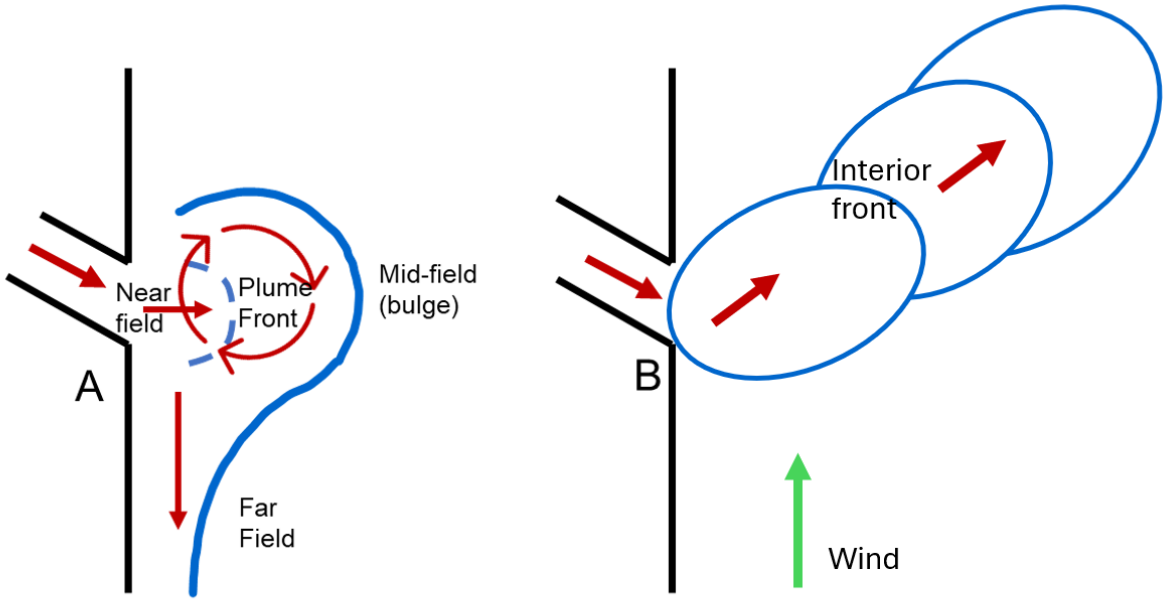

Figure 1. (a) a prototypical plume, and (b) a "cross-shelf" plume as influenced by sustained upwelling-favorable winds.

1.3 Objectives

As a result of plume tendency to export nutrients onto the shelf, numerous studies have been conducted on nutrient availability through river plume systems. A study conducted by Choisnard et al. (2024), investigated the variations in nitrification rates along the Amazon River Plume. This study found the highest amounts of DIN and the highest nitrification rates occurred nearest the river mouth and decreased with distance from the source as the freshwater mixed with ambient water. Additionally, a study conducted by Gomes et al. (2018b), on the partitioning of phytoplankton communities in two plume systems, found that DIN concentrations in the waters of the Amazon River Plume were highest at the source region and nearly depleted almost everywhere else; however, PO_4^{3-} increased with distance from the source region. They found that this decreasing N:P ratio

had a significant influence on the biodiversity and biomass of the phytoplankton in these waters. Another, a study conducted by Tong et al. (2023), investigated the dynamics and drivers of phytoplankton biomass in the Pearl River plume located in the South China Sea. This study found that the concentrations of DIN decreased from the low salinity plume to the high salinity plume while the dissolved inorganic phosphorous (PO_4^{3-}) remained relatively consistent. As a result, the plume waters transitioned from being P limited to N limited as the plume evolved. This shift gave rise to a change in dominating phytoplankton species. In addition to these more general studies, prior work has examined the availability of nutrients specifically at plume fronts. Franks, (1992), found an accumulation of phytoplankton species at convergent frontal boundaries. These results were further confirmed by the works of Li et al. (2022), who used a hydrodynamic model to show how the development of a transport barrier at frontal structures led to the accumulation of materials and prevented ambient waters from influencing the near field region.

Previous studies by Yankovsky et al. (2022) and Yankovsky & Voulgaris, (2019) have explored the physical dynamics of the WBP but have not examined nutrient distribution within this system. This study seeks to build on these previous works by exploring the distribution of nutrients in various regions of the WBP to increase understanding of how the development of a cross-shelf plume may impact primary productivity along the coast. Over the course of this project two hypotheses were developed based on the results of the previously described works.

Hypothesis 1 (H1): The concentrations of DIN and PO_4^{3-} will vary across plume regions. Specifically, the concentration of DIN will decrease and PO_4^{3-} will increase with distance from the estuary mouth and source region.

Hypothesis 2 (H2): There will be a significant accumulation of nutrients at the plume fronts with the highest concentrations recorded on the estuarine side of the fronts.

H1 is addressed using salinity, temperature, plume depth and Froude number calculations. These values act as indicators of the plume region along a transect of the WBP. H2 is addressed using data collected at two frontal structures. Each front was separated into an ocean side and an estuary side which could be visually distinguished by a sharp color gradient. The procedures for collecting the data and the analysis methods used to address these hypotheses are further discussed in section 2.

2 Methods

2.1 Study Site

Winyah Bay, pictured in Figure 2, is a partially mixed microtidal estuary that experiences predominantly semi-diurnal tides (Kim & Voulgaris, 2005) and an average tidal velocity of roughly 1 m/s (CO-OPS, 2024). This estuary is located on the South Atlantic Bight (SAB). The SAB is a shallow continental shelf on the east coast of the United States and has a shelf break that sits more than 100 km offshore (Yankovsky et al., 2022). The WBP is the largest outflow within the SAB due to the combination of the estuary shape and number of rivers that feed into the plume (Yankovsky et al., 2022). These rivers include the greater and lesser PeeDee, Waccamaw, Sampit, and Black rivers

Figure 2. Satellite image of Winyah Bay, located in Georgetown, South Carolina (red star). Attribution: Esri, HERE, Garmin, SafeGraph, GeoTechnologies, Inc, MET/NASA, USGS, EPA, NPS, US Census Bureau, USDA.

2.2 Data Collection

2.2.1 Cruise Logistics

Data were collected on the *R/V Savannah* from April 10- 16, 2023. Water samples were collected from 6 transects which are outlined in Table 1. To address the first hypothesis of this study, data collected from transect N (Figure 3) were used. This transect was designed to cut along the length of the plume with the intention of gathering data across a range of plume regions, moving away from the source. This transect consisted of 21 (N1 to N21) stations with 1 nautical mile spacing. Water samples, however, were only collected at stations N1-N7 due to limited sample bottles. To address the second hypothesis of this study, data collected around two fronts, at stations F and TS1 (Figure 3), were used. F1 and TS1c were located on the estuarine side of their respective fronts and F3 and TS1a were on the ocean side. Additionally, data were collected at station O1 to be used as a reference for ambient ocean conditions. Stations O and F were visited the morning of April 12th, station TS1 sampling was the morning of April 13th, and transect N sampling was early afternoon on April 14th. Furthermore, discharge rates measured at in the PeeDee river, the largest inflow to Winyah Bay, steadily rose from about 460 m^3/s on April 10th, to roughly 830 m^3/s on April 15th (USGS, 2024). At the beginning of the cruise winds were blowing to the southwest but changed to light upwelling favorable conditions, blowing to the northeast the morning of April 14th around 7 o'clock (local time).

Table 1. Transect information including date and time, total number of stations, stations where water was collected, and description of why transect was sampled.

Date/Time (local)	Transect	Total number of stations	Stations samples were collected	Description
4/12: 8:44	O	1	O1	Ocean Reference
4/12: 11:00 – 11:10	F	3	F1, F3	Interior front: Oceanside (F3), Estuarine side (F1)
4/12: 13:07 – 18:35	P	26	P1, P4, P7, P8	Cut along plume
4/13: 9:25 - 11:06	TS1	3	TS1a, TS1c	Time series across front: Oceanside (TS1a), Estuarine side (TS1c)
4/13: 13:35	B	17	B1a	Box around section of plume
4/14: 15:11 – 19:40	N	21	N1-N7	Nutrients transect along plume

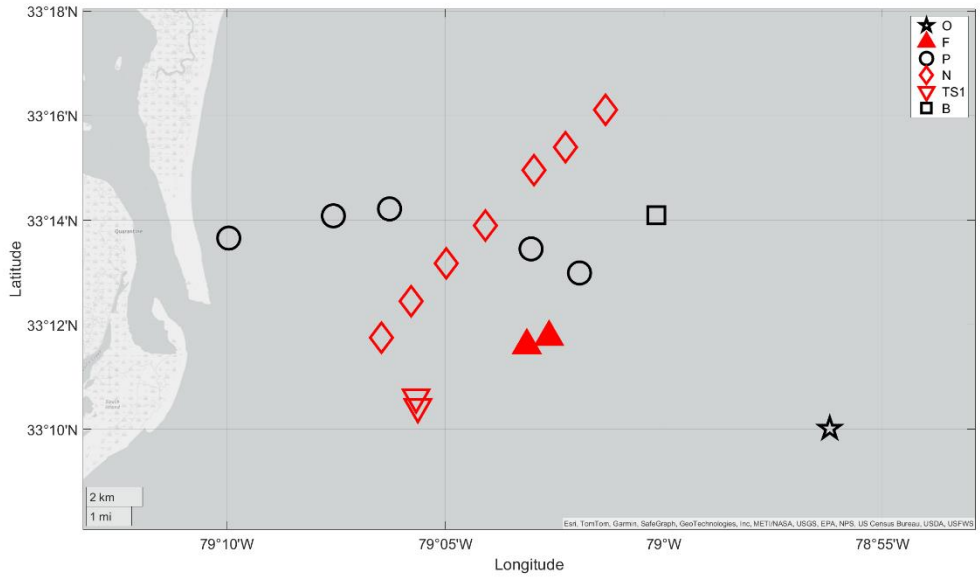

Figure 3. Map of stations sampled in April 2023 where water was collected.

2.2.2 Water Sample Collection

Prior to field work a series of 25 ml sample bottles were prepared by acid washing in 10% HCL, followed by rinsing with MilliQ water. Water was collected via Niskin bottles attached to a CTD rosette, sampling across the first 2 m of the water column based on the size of the Niskin bottles. This depth maximized the chances of sampling within the plume and was as close to the surface as the rosette allowed. At each station, 3 replicates (A, B, and C) were obtained, except for station N7 which had 2 replicates. The replicates for each station were taken from the same Niskin bottle except for line N whose replicates were taken from separate bottles. After being filled, the bottles were labeled with station and replicate before being frozen until further processing could occur in the lab. A total of 50 samples were collected during this trip

2.2.3 Supplementary Data Collection

A SBE 911plus/917plus CTD collected temperature, salinity, density, dissolved oxygen, chlorophyll fluorescence, pH, and turbidity measurements at each station. A VMP 250 (Rockland Scientific) and a microCTD (Rockland Scientific) also collected temperature and salinity measurements. The VMP 250, which also provides turbulent kinetic energy (TKE) dissipation estimates, was deployed 3 times at each station. Due to the structure of this instrument, measurements did not begin until roughly 1 m in depth, whereas the upward profiling microCTD provided measurements much closer to the surface. Additionally, the R/V Savannah was equipped with a flow through system that continuously measured near-surface water properties including temperature, salinity, and chlorophyll concentrations.

Velocity measurements were collected using a ship ADCP (1200 kHz hull mounted).

This instrument started collecting measurements at a depth of 3.1 m below the surface and collected data continuously through the entirety of the cruise. Additionally, a RoboCat AD2CP (Nortek signature 1000 profiler) was also used in April to collect water velocity data. This ADCP (1000kHz), mounted to an autonomous surface vehicle known as the RoboCat, was designed to collect data at a distance from the boat while loitering within a fixed radius. This was done to minimize the interference from the vessel on the velocity data. The RoboCat, which was deployed at each station, collects measurements close to the surface (0.45m) during bursts that last 6 minutes.

2.3 Data Processing

2.3.1 Density

The salinity and temperature measurements collected by the VMP and MicroCTD were used to calculate the in-situ density profiles at each station. The densities were then extended up to the surface assuming constant values from the shallowest measured point to the surface. This assumption is reasonable if the shallowest data point is within the surface mixed layer, or within a well-mixed plume. For the microCTD data extrapolation is over a relatively small region, however for the VMP this extrapolation may extend up to 2 m depth, which means that the approximation is more accurate for the microCTD.

2.3.2 Plume Depth

The plume depth (Equation 1) was calculated at each station using the calculated density profiles. The plume depth equation employed in this study, derived from the work of (Arneborg et al., 2007) is expressed as

$$D = \frac{2\int_{-h}^{0} \frac{\rho(z)-\rho_o}{\rho_o}\, z\, dz}{\int_{-h}^{0} \frac{\rho(z)-\rho_o}{\rho_o}\, dz} \qquad (1)$$

where, z represents the water depth at a specific point and h is the total water depth, $\rho(z)$ signifies the water density at a given depth, and ρ_o represents the ambient water density. For this study the maximum density at each station was used to represent the ambient water conditions. After the calculations were completed the plume depth was then used to calculate averaged parameters within the plume layer including dissolved oxygen, chlorophyll fluorescence, salinity, and temperature.

2.3.3 Froude Number

The Froude number (Equation 2) is a non-dimensional number used to evaluate the competing forces driving plume propagation, which illustrates the competition of the inertial momentum of flow and the velocity driven by the density difference between the plume and the underlying waters. A plume is considered to be supercritical when $Fr > 1$, often associated with the near field (Horner-Devine et al., 2015). It is defined as(Horner-Devine et al., 2015):

$$Fr = \frac{V}{\sqrt{g'D}} \qquad (2)$$

Where V represents the plume's velocity magnitude ($V = \sqrt{u^2 + v^2}$). Here u and v denote the eastward and northward velocity components, respectively. The velocity components were integrated from the plume depth to the surface. The calculation of $g'D$ follows the approach of Arneborg et al. (2007) using Equation 3 below.

$$g'D = \int_{-h}^{0} g \frac{\rho(z) - \rho_0}{\rho_0} dz \qquad (3)$$

Where g is the gravitational constant 9.81 m/s^2.

2.3.4 Nutrients

Post-cruise, all frozen samples were thawed, then analyzed for NO_3^-, NO_2^-, NH_4^+, and PO_4^{3-}. Concentrations of NO_3^- were determined using the methods set forth by Schnetger & Lehners, (2014). The methods for determining NO_2^- concentrations were provided by Bendschneider & Robinson, (1952). Analysis of NH_4^+ concentrations was completed using the methods of Holmes et al., (1999). The concentrations of NO_3^-, NO_2^-, and NH_4^+ were summed to calculate the total DIN. Lastly, PO_4^{3-} concentrations were analyzed using the methods delineated by Murphy & Riley, (1962).

2.4 Data Analysis

2.4.1 The Linear Models

To test H1, a series of scatter plots were examined to visualize any potential linear relationships among the variables. Subsequently, two multiple linear regression analyses were conducted: one analyzing DIN in relation to the predictor variables (salinity, temperature, plume depth, and Froude number), and the other focusing on PO_4^{3-} and the same predictor variables. Given the spatial nature of the data, each regression model was evaluated using Rao's test to assess any potential spatial autocorrelation. Furthermore, this test was used to determine whether a spatial error model or spatial lag model would better account for the spatial aspect of the data and enhance the original regression model.

2.4.2 The Plume Fronts

To evaluate H2, the frontal data was categorized into an ocean side (TS1a and F3) and an estuarine side (TS1c and F1). These data were then represented using separate jitter plots for DIN and PO_4^{3-}, effectively visualizing their central tendencies. Given the small sample size, the Wilcoxon Rank Sum test was employed to compare the location of the two

populations. Consequently, median was used as the measure of central tendency.

3 Results

3.1 Data visualization

Figure 4 illustrates the distribution of average DIN (a) and PO_4^{3-} (b) along transect N in spatial coordinates. The highest concentration of DIN across the transect was observed at station N3 (2.02 µmol/L) and the second highest at station N7 (1.97 µmol/L), whereas the lowest DIN concentration was observed at station N5 (0.71 µmol/L). Furthermore, PO_4^{3-} reached the highest concentration at station N5 (0.16 µmol/L) and the lowest PO_4^{3-} concentration at station N7 (0.069 µmol/L).

Notably, the estuarine side of the frontal stations (F1 and TS1c) exhibited peak DIN concentrations exceeding 3.25 µmol/L each, whereas the ocean reference station (O1) displayed the lowest overall DIN concentration of 0.18 µmol/L. Comparatively, PO_4^{3-} concentrations surpassed 0.23 µmol/L at the estuarine frontal stations, whereas the lowest overall PO_4^{3-} concentration was recorded at station O1 with a value of 0.019 µmol/L. Nutrient concentration values across the entirety of the trip are provided in Table 2.

Conservative mixing plots (Figure 5a and 5b) illustrate further trends in DIN and PO_4^{3-} concentrations. Salinity serves as a tracer for the expected nutrient concentration within this system. The dashed black line represents the conservative mixing line, it connects the least and most saline points in a system, reflecting the anticipated nutrient concentration under ideal conservative mixing conditions within the plume.

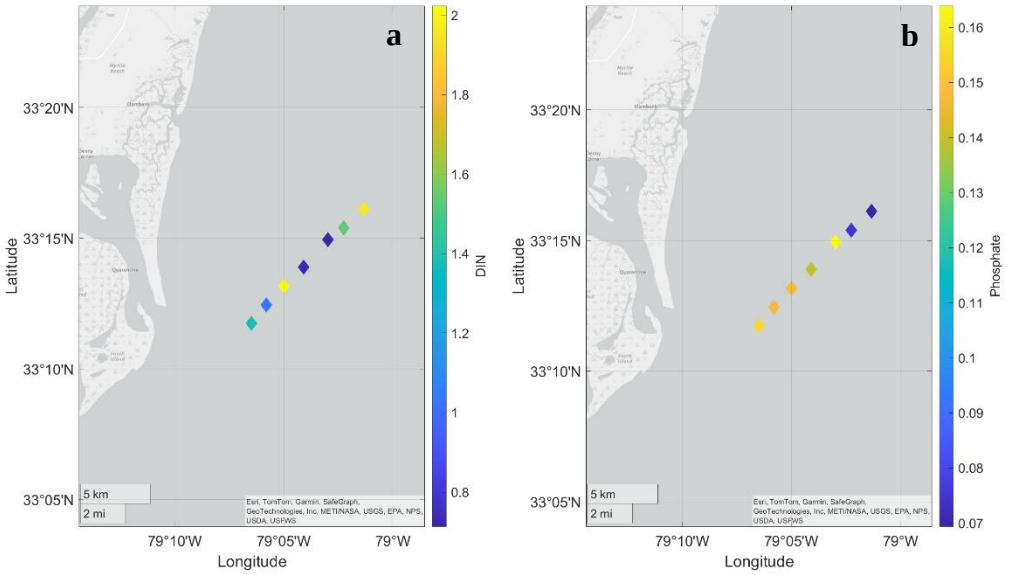

Figure 4. (a) map of average DIN concentrations in µmol/L along transect N. (b) map of average PO_4^{3-} concentrations in µmol/L along transect N.

Table 2. The average DIN and PO_4^{3-} concentrations calculated from the 3 replicates at each station for the entire cruise and 1 standard deviation (SD).

Station	[DIN] (µmol/L)	SD (+/-)	[PO_4^{3-}] (µmol/L)	SD (+/-)
O1	0.177	0.125	0.019	0.018
F1	3.817	0.124	0.232	0.032
F3	1.594	0.207	0.104	0.018
P1	0.305	0.002	0.108	0.030
P4	0.988	0.014	0.166	0.111
P7	0.806	0.037	0.112	0.012
P8	1.260	0.134	0.152	0.007
TS1a	1.364	0.092	0.200	0.014
TS1c	3.253	0.117	0.305	0.044
B1a	0.594	0.024	0.087	0.012
N1	1.379	0.258	0.156	0.025
N2	1.030	0.256	0.148	0.048
N3	2.023	1.479	0.148	0.000
N4	0.733	0.164	0.140	0.073
N5	0.713	0.166	0.164	0.046
N6	1.537	0.291	0.075	0.000
N7	1.971	0.089	0.069	0.009

In Figure 5a, DIN concentrations consistently exceeded the conservative mixing line, indicating an overall input of DIN into this system. Likewise, Figure 5b shows that the majority of the PO_4^{3-} concentrations lie above the line, suggesting an input of PO_4^{3-} into the system, while a few concentrations fall below the line, indicating potential removal processes.

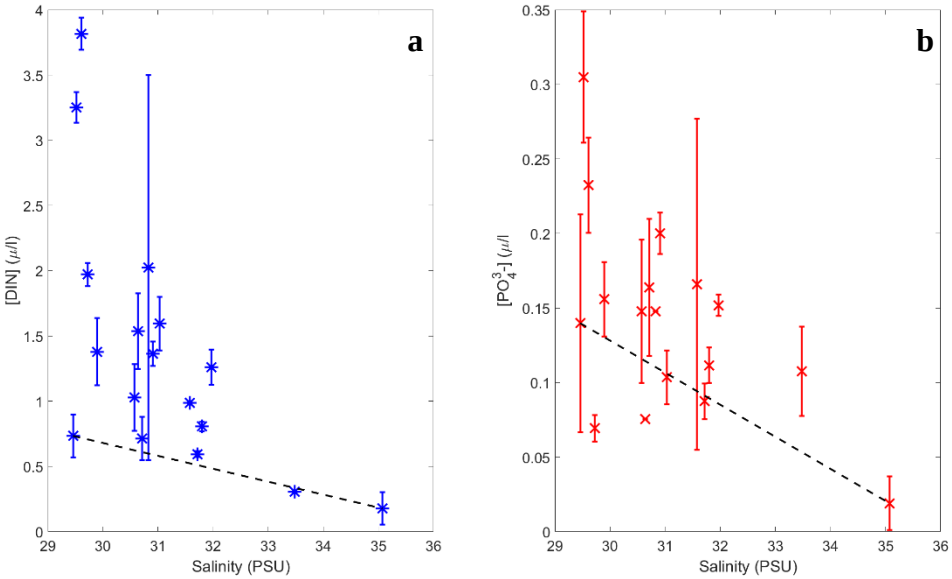

Figure 5. Conservative mixing plots for DIN (left) and PO_4^{3-} (right). The black dashed line represents the conservative mixing line.

Salinity and temperature contours generated from the profiles taken along transect N are presented in Figure 6. Surface salinity values exhibited a gradual increase from station N1 to N7, whereas surface temperatures decreased along the same transect. Measurements at stations N1-N4 were obtained using an upward profiling microCTD, capturing data closer to the sea surface compared to the downward profiling VMP used at stations N5-N7, thereby explaining the lack of near-surface data at the latter stations. Both Figures 6a and 6b illustrate a distinct gradient between warmer, fresher water and cooler, saltier water.

The plume depth, delineated by the dashed red line, closely follows this gradient. As depicted in Figure 6 the plume depth deepens in a stepwise fashion with increasing distance from station 1, consistent with the findings of (Yankovsky & Voulgaris, 2019).

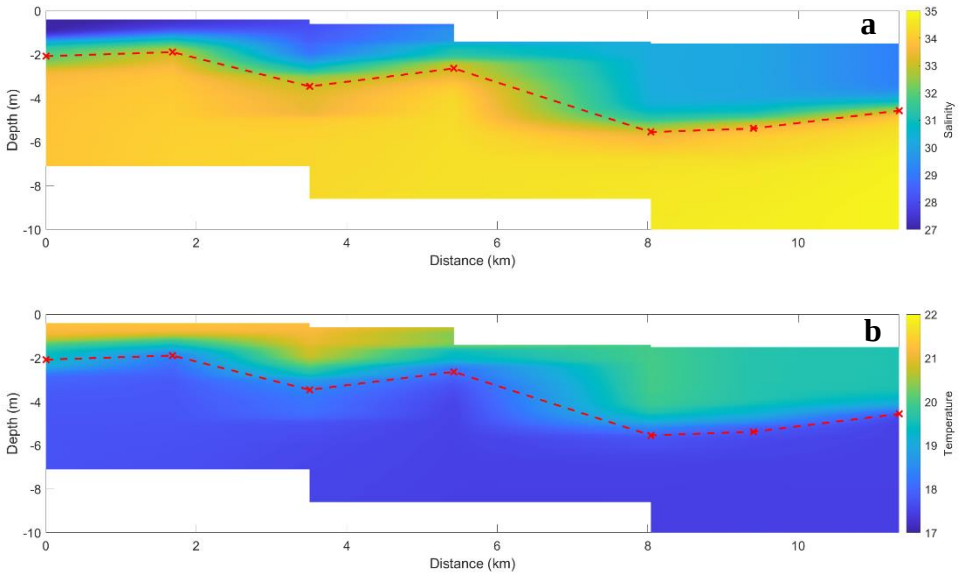

Figure 6. (a) salinity profile along transect N collected April 2023. (b) temperature profile along transect N collected April 2023. The dashed red line indicates the plume depth at each station marked with a red X.

The Froude number (Equation 2) is depicted in Figure 7. The red line represents the traditional threshold for identifying supercritical flow (Fr > 1). Stations N1 and N2 exceed this threshold, indicating supercritical flow and placing these stations in the nearfield region. Stations N3 to N7 exhibit values below this threshold, decreasing relatively consistently. This indicates that advection momentum is becoming less important further from the source, and other forces, including Ekman transport or geostrophic flow, may be gaining in influence.

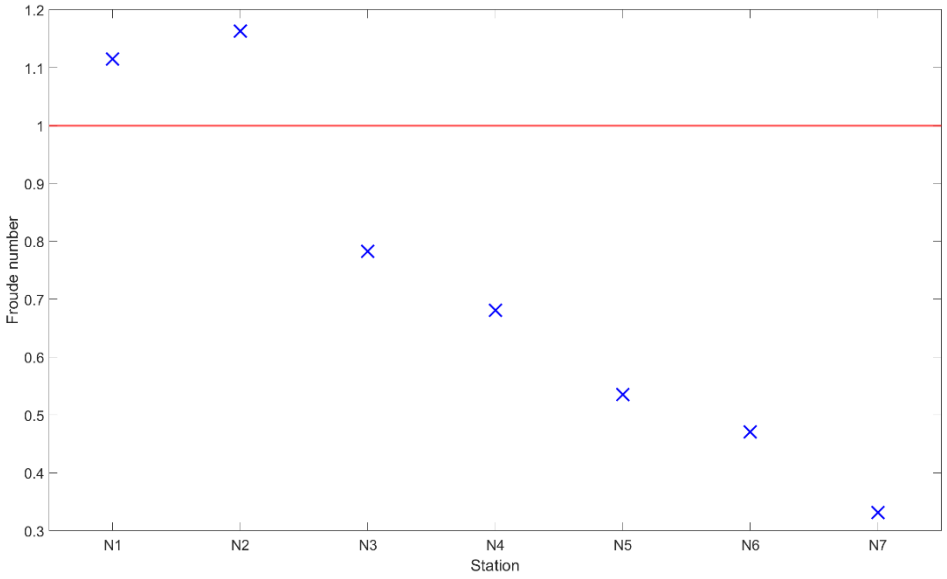

Figure 7. The Froude number across transect N calculated with Equation 2 using data collected in April 2023.

3.2 Hypothesis 1

Due to small sample sizes, fitting multiple linear regression models including all the plume region variables (salinity, temperature, plume depth, and Froude number) to the data was not reasonable. Therefore, a simplified multiple linear regression was performed using only temperature and salinity as predictors for both PO_4^{3-} and DIN. These reduced models similarly concluded that neither temperature nor salinity significantly predicted DIN or PO_4^{3-} levels either with the spatial lag and spatial error models or without.

Furthermore, simple linear regressions were conducted for each individual predictor variable against PO_4^{3-} and DIN. In each instance the models resulted in p-values greater than 0.05, consistent with the reduced multiple linear regressions. This once again indicates there is minimal evidence that salinity, temperature, plume depth, or Froude number serve as important predictors of PO_4^{3-} or DIN in this study.

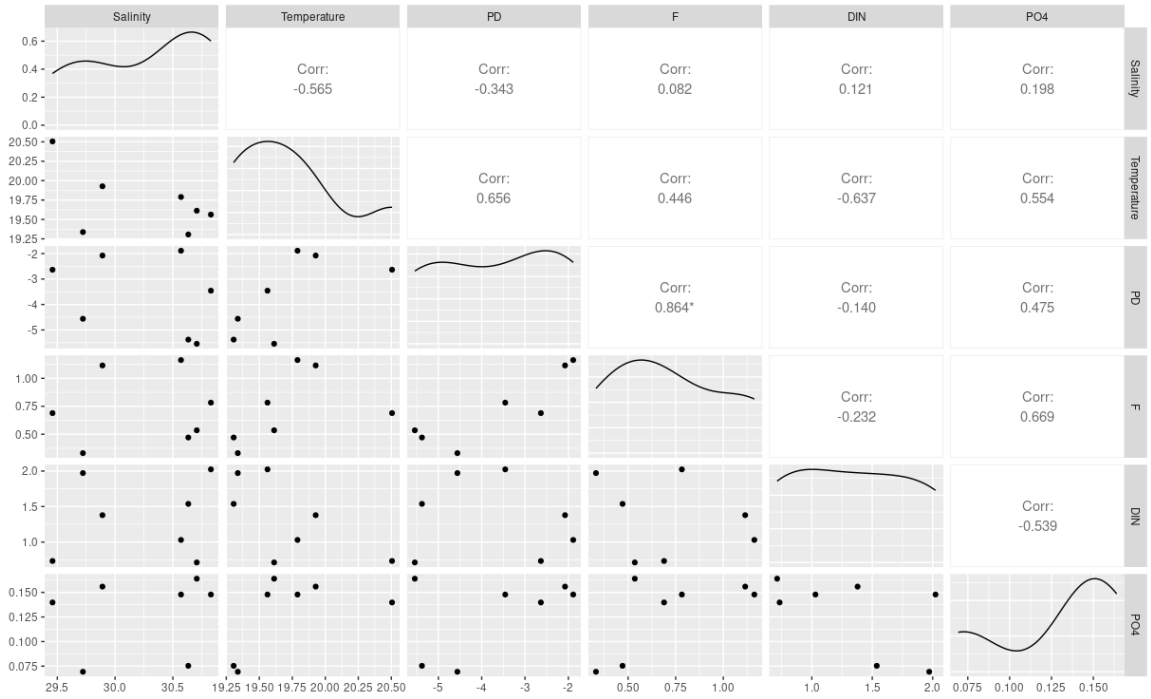

Figure 8. Scatter plots comparing the response variable (DIN and PO_4^{3-}) to the predictor variable (salinity, temperature, plume depth, and Froude number)

The results reported above used temperature and salinity values averaged over the plume depth. As these data did not produce significant results, the model was also run using temperature and salinity as close to 1 m depth as possible, to better correspond with the depth of water collection. Results of this analysis were consistent with those above. There was little to no evidence suggesting that any of the plume region variables significantly predicted PO_4^{3-} and DIN levels in this investigation. Table 3 and table 4 provide a full overview of the results from each analysis completed for H1.

Table 3. Results of the multiple linear regression or simple linear regression, spatial lag, and spatial error models completed using DIN as a response. Salinity/Temperature type indicates whether the averaged (Ave) or 1 m (Surface) salinity and temperature measurements were used.

Predictor(s)	Salinity/Temperature type	Linear regression (p-value)	Spatial lag (p-value)	Spatial error (p-value)
Salinity/Temperature	Ave	0.261300	0.476900	0.899600
Salinity/Temperature	Surface	0.343800	0.582810	0.602140
Salinity	Ave	0.795300	0.814100	0.819600
Salinity	Surface	0.329100	0.941100	0.723100
Temperature	Ave	0.124100	0.683000	0.664100
Temperature	Surface	0.926500	0.832500	0.806500
Plume Depth	-	0.764200	0.797000	0.824700
Froude Number	-	0.616700	0.761000	0.844200

Table 4. Results of the multiple linear regression or simple linear regression, spatial lag, and spatial error models completed using PO_4^{3-} as a response. Salinity/Temperature type indicates whether the averaged (Ave) or 1 m (Surface) salinity and temperature measurements were used.

Predictor(s)	Salinity/Temperature type	Linear regression (p-value)	Spatial lag (p-value)	Spatial error (p-value)
Salinity/Temperature	Ave	0.095760	0.163500	0.811000
Salinity/Temperature	Surface	0.072270	0.626840	0.369470
Salinity	Ave	0.670400	0.212400	0.208500
Salinity	Surface	0.504300	0.285600	0.381400
Temperature	Ave	0.196800	0.514800	0.791700
Temperature	Surface	0.058110	0.766200	0.948300
Plume Depth	-	0.280900	0.511900	0.920900
Froude Number	-	0.100000	0.697200	0.830200

3.3 Hypothesis 2

There was a significant difference in the DIN and PO_4^{3-} concentrations observed between the estuarine and ocean sides of the fronts (F and TS1), as shown in Figure 9a and

9b. The unaveraged nutrient data was used to address H2, thus each side was comprised of 6 data points. This was because there were only two frontal structures sampled during the cruise period and using the unaveraged data allowed for a large enough dataset to complete analysis.

DIN concentrations on the estuarine side of the front ranged from 3.18 µmol/L to 3.95 µmol/L, with a median of 3.55 µmol/L, and from 1.26 µmol/L to 1.82 µmol/L, with a median of 1.42 µmol/L on the ocean side. The Wilcoxon Rank Sum test provided very strong statistical evidence ($p < 0.01$) that the concentrations of DIN were significantly higher on the estuarine sides compared to the ocean sides (Figure 9a).

Additionally, PO_4^{3-} concentrations ranged from 0.20 µmol/L to 0.34 µmol/L, with a median of 0.26 µmol/L on the estuarine side and ranged from 0.09 µmol/L to 0.18 µmol/L, with a median 0.15 µmol/L on the ocean side. Despite a narrower difference in PO_4^{3-} concentrations between the estuarine and ocean sides (Figure 9b), the Wilcoxon Rank Sum test still resulted in strong statistical evidence ($p < 0.05$) that the PO_4^{3-} concentrations are significantly higher on the estuarine sides of the fronts.

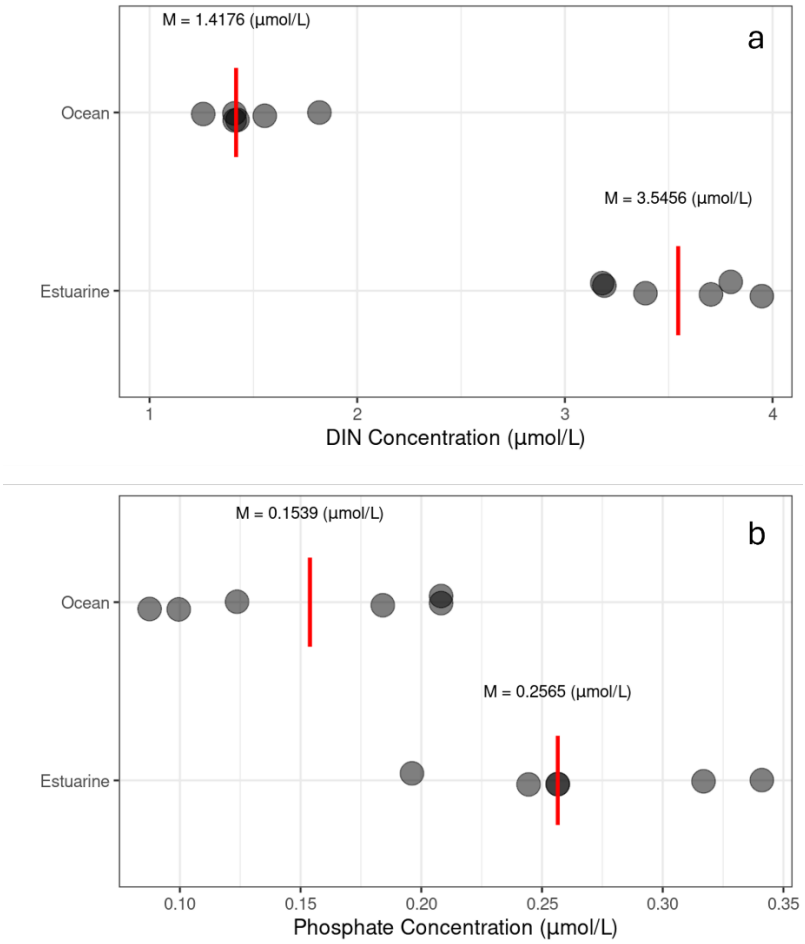

Figure 9. Jitter plots comparing the concentrations of DIN (a) and PO_4^{3-} (b) on the estuarine and ocean sides of the fronts observed in April 2023.

4 Discussion

4.1 Hypothesis 1

The analyses in this study revealed no significant linear trends in the concentrations of DIN or PO_4^{3-} with the chosen forcing factors. There is a possibility that the limited sample size makes it difficult to observe any relationships between DIN and PO_4^{3-} with the variables characterizing plume regions. Figure 10a and 10b depict temperature-salinity diagrams utilizing all stations (not just line N) for DIN and PO_4^{3-}, respectively, highlighting potential correlations that may become apparent with a larger data set. Observational trends indicate higher concentrations of DIN and PO_4^{3-} tend to cluster in the lower left corners of the graphs, suggesting cooler and fresher water may harbor higher nutrient levels. However, caution must be exercised when interpreting these observations, as the data were collected over several days across a broad spatial extent, introducing various influencing factors.

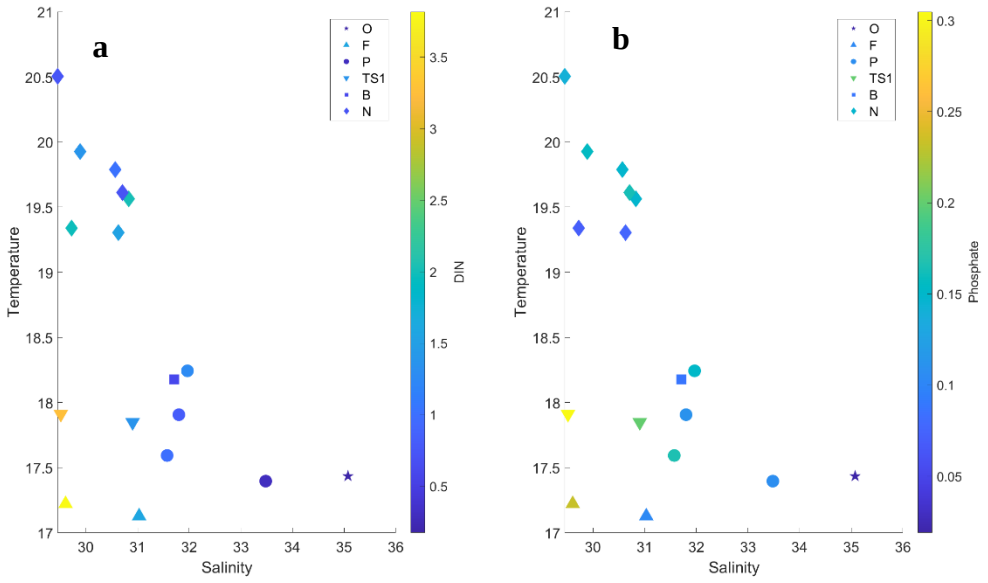

Figure 10. T-S diagrams of DIN (a) and PO_4^{3-} (b) in µmol/L at every station sampled during the April 2023 cruise

The behavior of DIN concentrations in this study diverged from expected patterns. Unlike the findings of Gomes et al. (2018b) and Choisnard et al. (2024), who observed peak DIN concentrations at the source region with depletion elsewhere, DIN levels in transect N exhibited highest concentrations at the middle and end stations. Similarly, PO_4^{3-} concentrations showed unexpected trends compared to previous studies, decreasing with distance from the source rather than increasing as reported by Gomes et al. (2018b). Not only was there a lack of relationships with distance from the source, but the trends could not be explained by patterns in salinity, temperature, plume depth, or Froude number. This discrepancy suggests the presence of additional, unaccounted-for factors influencing DIN and PO_4^{3-} concentrations in the plume system.

Further supporting this observation are the conservative mixing plots (Figure 5), indicating that these dissolved nutrients are being added to the system at a rate faster than they are being removed, possibly indicating reduced photosynthetic activity and enhanced respiration, compared to earlier studies. Relative levels of primary productivity can be evaluated by examining trends in chlorophyll fluorescence, as measured by the CTD. Additionally, dissolved oxygen (DO) can also act as a proxy of biological activity by using percent saturation as an indicator of the balance between oxygen production and consumption. Figure 11a and 11b depict maps of surface dissolved oxygen and chlorophyll concentrations, respectively. Plot (a) reveals no discernible spatial patterns in dissolved oxygen concentrations, which aligns with expectations given its susceptibility to atmospheric mixing and biological influences. This could also explain the lack of correlation between dissolved oxygen and the two nutrient constituents (Figure 12). In contrast, the chlorophyll map (b) shows a trend where lower concentrations are observed

at the beginning of the transect, and higher values occurring towards the middle.

When comparing chlorophyll concentrations to PO_4^{3-} and DIN (Figure 13) there were no strong correlations. These results are unlike those of Lohrenz et al. (1999) who found a non-conservative depletion of nutrients, including DIN and PO_4^{3-}, when chlorophyll was at its maximum. In this study, a simple linear regression, performed on both DIN and PO_4^{3-}, did not provide any statistical evidence ($p > 0.05$) that chlorophyll is an important indicator of DIN and PO_4^{3-} levels. This directly contradicts the literature; however, the results of the limited sample size may prevent drawing definitive conclusions from these observations.

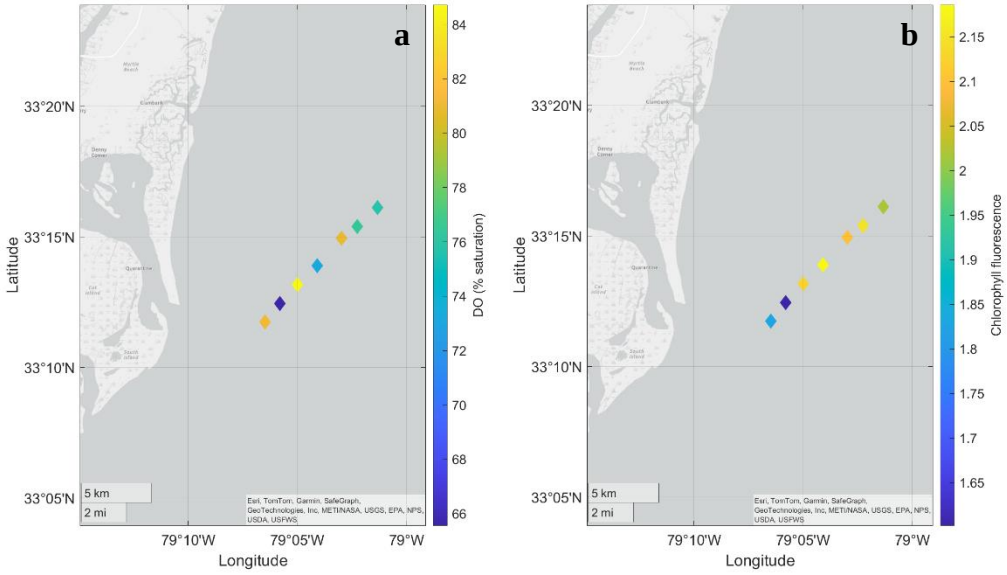

Figure 11. Maps of surface dissolved oxygen percent saturation (a) and chlorophyll fluorescence (b) over transect N collected via CTD in April 2023.

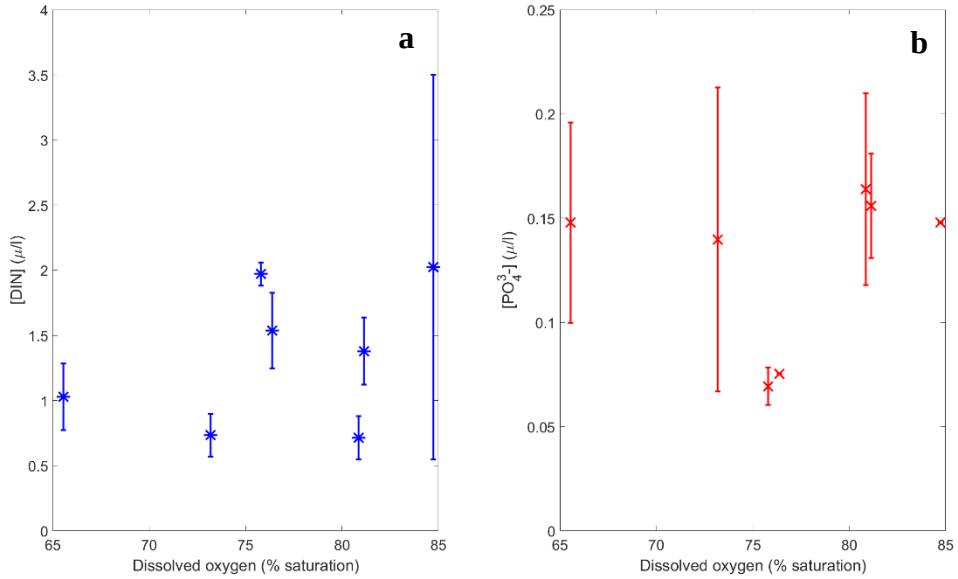

Figure 12. Concentrations of DIN (a) and PO_4^{3-} (b) compared to dissolved oxygen (percent saturation) for transect N.

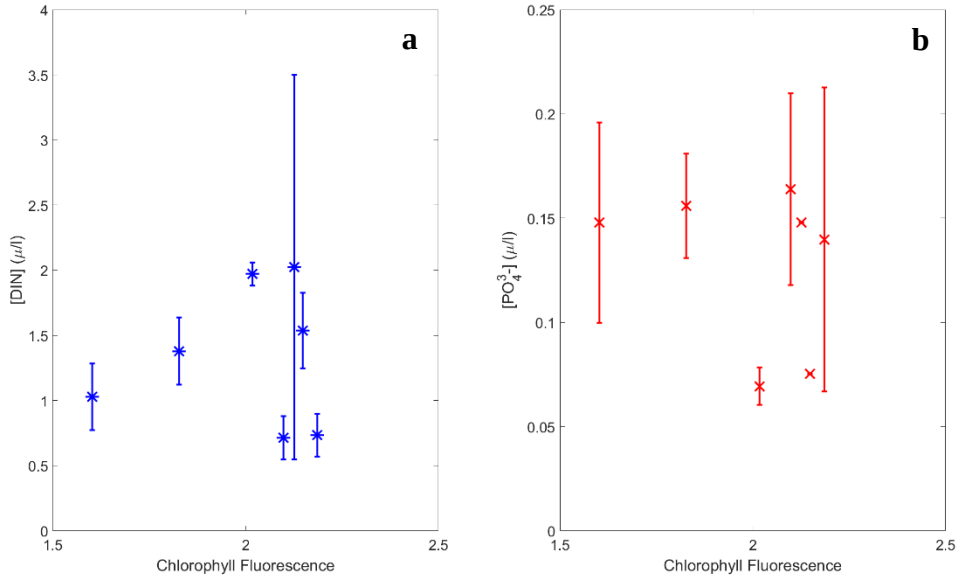

Figure 13. Concentrations of DIN (a) and PO_4^{3-} (b) compared to chlorophyll fluorescence for transect N.

Alternatively, the spikes in DIN observed at stations N3 and N7 could be attributed to advective processes, where DIN from deeper waters is transported upwards, consistent with

findings by Han et al. (2012), who observed elevated DIN concentrations in upwelled waters compared to plume waters in the South China Sea. During this cruise wind conditions were blowing towards the southwest until the morning of the 14th when they switched to a light upwelling favorable wind. These wind conditions could cause upwelling that potentially explains the high concentrations of DIN at stations N3 and N7. Furthermore, surface winds can enhance ocean-atmosphere oxygen exchange potentially explaining the lack of patterns between dissolved oxygen levels and the nutrient concentrations.

These findings bring to light the complex relationships of factors influencing nutrient dynamics in the WBP system, highlighting the need for further investigation. Future analysis would benefit from a larger dataset to further clarify the relationships between these factors. Additionally, future investigations could include measurements at the bottom of or below the plume to address any questions regarding advection from deeper waters' influence on nutrient concentrations at the surface.

4.2 Hypothesis 2

This study's findings present statistical evidence that concentrations of DIN and PO_4^{3-} are significantly elevated on the estuarine sides of the fronts compared to the ocean sides. This accumulation pattern aligns with previous research by Franks (1992) and Li et al. (2022), highlighting the tendency for nutrients to accumulate prominently on the estuarine side of fronts. Notably, these stations consistently exhibited the highest concentrations of both DIN and PO_4^{3-} throughout the entire research cruise, illustrating the importance of these structures in context of biological productivity. Additionally, nutrient concentrations on both sides of the visible front occasionally exceeded the concentrations of DIN and

PO_4^{3-} observed along transect N, indicating that frontal convergence potentially contributes to nutrient accumulation on both sides.

Previous studies in the Winyah Bay plume have focused on physical dynamics that can be measured with a variety of automated and acoustic techniques. However, collecting nutrient data requires more intensive sampling, including collecting water samples at specific depths in the field, preserving samples for analysis, and bench work to process the samples for nutrient concentrations. This limiting factor, along with the transient nature of the plume, makes collecting a comprehensive dataset challenging. However, this study has shown the value of collecting said data set, as a relatively large dataset is needed to resolve the spatial variability in these systems. Furthermore, these results highlight the importance of investigating how nutrient concentrations evolve within individual fronts as they propagate away from their source regions. This avenue of research could provide valuable insights into the dynamics of nutrient transport and accumulation in coastal environments.

5. Conclusion

River plumes are incredibly influential systems. The materials and particulates they transport exert significant influence on coastal ecosystems, shaping them both physically and biologically. However, these systems are highly dynamic and constantly evolving, making it challenging to understand the complicated relationships between nutrient concentrations and various plume variables. This study aimed to enhance our understanding of nutrient dynamics within these systems, specifically how nutrient concentrations are distributed across different plume regions and their implications for biological activity.

This study produced unexpected findings. Nutrient concentrations peaked at the fronts, particularly at the estuarine side, consistent with initial hypotheses. These high concentrations indicate that the convergent nature of these frontal structures provide high levels of accumulation on both sides, thus, making these structures potentially important features for primary production and nutrient delivery. However, contrary to expectations, both DIN and PO_4^{3-} concentrations exhibited no discernible trends along the plume (transect N). It was anticipated that DIN would decrease with distance from the mouth, and PO_4^{3-} would increase. However, these anticipated trends were not observed, and no significant correlations emerged between the nutrient concentrations and plume region variables. These results suggest that factors beyond those initially considered, such as biological activity or advection, may play a predominant role in influencing DIN and PO_4^{3-} concentrations within these systems

Despite efforts to understand these concepts, this study encountered limitations due to a small sample size, potentially preventing definitive conclusions regarding which regions are likely to harbor the highest nutrient concentrations. The dynamic nature of river plumes highlights the need for future investigations to delve deeper into these systems. Further research in this area is essential for gaining a comprehensive understanding of nutrient dynamics in river plumes and their implications for coastal ecosystem health.

6. References

Arneborg, L., Fiekas, V., Umlauf, L., & Burchard, H. (2007). Gravity current dynamics and entrainment - A process study based on observations in the Arkona Basin. *Journal of Physical Oceanography*, *37*(8), 2094–2113. https://doi.org/10.1175/JPO3110.1

Bendschneider, K., & Robinson, R. J. (1952). *A New Spectrophotometric Method for the Determination of Nitrate is Sea Water*.

Beusen, A. H. W., Bouwman, A. F., Van Beek, L. P. H., Mogollón, J. M., & Middelburg, J. J. (2012). Global Riverine N and P Transport to Ocean Global Riverine N and P Transport to Ocean Increased During the Twentieth Century Despite Increased Retention Along the Aquatic Continuum Global Riverine N and P Transport to Ocean. *Biogeosciences Discuss*, *12*. https://doi.org/10.5194/bgd-12-20123-2015

Bouwman, A. F., Van Drecht, G., Knoop, J. M., Beusen, A. H. W., & Meinardi, C. R. (2005). Exploring changes in river nitrogen export to the world's oceans. *Global Biogeochemical Cycles*, *19*(1), 1–14. https://doi.org/10.1029/2004GB002314

Cai, W. J., Hu, X., Huang, W. J., Murrell, M. C., Lehrter, J. C., Lohrenz, S. E., Chou, W. C., Zhai, W., Hollibaugh, J. T., Wang, Y., Zhao, P., Guo, X., Gundersen, K., Dai, M., & Gong, G. C. (2011). Acidification of subsurface coastal waters enhanced by eutrophication. *Nature Geoscience*, *4*(11), 766–770. https://doi.org/10.1038/ngeo1297

Choisnard, N., Sperlea, T., Liskow, I., & Voss, M. (2024). Nitrification in the Amazon River plume. *Marine Ecology Progress Series*, *730*, 1–14. https://doi.org/10.3354/meps14530

Cloern, J. (2001). Our Evolving Conceptual Model of the Coastal Eutrophication Problem. *Marine Ecology Progress Series*, *210*, 223–253.

Cole, K. L., & Hetland, R. D. (2016). The effects of rotation and river discharge on net mixing in small-mouth Kelvin number plumes. *Journal of Physical Oceanography*, *46*(5), 1421–1436.

https://doi.org/10.1175/JPO-D-13-0271.1

CO-OPS. (2024). *NOAA tidal current predictons*. https://tidesandcurrents.noaa.gov/

Franks, P. J. S. (1992). *Sink or swim: accumulation of biomass at fronts* (Vol. 82).

Galloway, J. N., Townsend, A. R., Erisman, J. W., Bekunda, M., Cai, Z., Freney, J. R., Martinelli, L. A., Seitzinger, S. P., & Sutton, M. A. (n.d.). *Transformation of the Nitrogen Cycle: Recent Trends, Questions, and Potential Solutions*. www.initrogen.org

Giraud, X., Le Quéré, C., & da Cunha, L. C. (2008). Importance of coastal nutrient supply for global ocean biogeochemistry. *Global Biogeochemical Cycles*, *22*(2). https://doi.org/10.1029/2006GB002717

Gomes, H. do R., Xu, Q., Ishizaka, J., Carpenter, E. J., Yager, P. L., & Goes, J. I. (2018a). The influence of Riverine Nutrients in Niche Partitioning of phytoplankton Communities-A contrast between the Amazon River Plume and the Changjiang (Yangtze) River Diluted Water of the East China Sea. *Frontiers in Marine Science*, *5*(SEP). https://doi.org/10.3389/fmars.2018.00343

Gomes, H. do R., Xu, Q., Ishizaka, J., Carpenter, E. J., Yager, P. L., & Goes, J. I. (2018b). The influence of Riverine Nutrients in Niche Partitioning of phytoplankton Communities-A contrast between the Amazon River Plume and the Changjiang (Yangtze) River Diluted Water of the East China Sea. *Frontiers in Marine Science*, *5*(SEP). https://doi.org/10.3389/fmars.2018.00343

He, G., Lao, Q., Jin, G., Zhu, Q., & Chen, F. (2023). Increasing eutrophication driven by the increase of phosphate discharge in a subtropical bay in the past 30 years. *Frontiers in Marine Science, 10*. https://doi.org/10.3389/fmars.2023.1184421

Holmes, R. M., Aminot, A., Kérouel, R., Hooker, B. A., & Peterson, B. J. (1999). *A simple and precise method for measuring ammonium in marine and freshwater ecosystems*.

Horner-Devine, A. R., Hetland, R. D., & MacDonald, D. G. (2015). Mixing and transport in coastal river plumes. In *Annual Review of Fluid Mechanics* (Vol. 47, pp. 569–594). Annual Reviews

Inc. https://doi.org/10.1146/annurev-fluid-010313-141408

Jickells, T. D., Buitenhuis, E., Altieri, K., Baker, A. R., Capone, D., Duce, R. A., Dentener, F., Fennel, K., Kanakidou, M., LaRoche, J., Lee, K., Liss, P., Middelburg, J. J., Moore, J. K., Okin, G., Oschlies, A., Sarin, M., Seitzinger, S., Sharples, J., … Zamora, L. M. (2017). A reevaluation of the magnitude and impacts of anthropogenic atmospheric nitrogen inputs on the ocean. *Global Biogeochemical Cycles*, *31*(2), 289–305. https://doi.org/10.1002/2016GB005586

Kilcher, L. F., & Nash, J. D. (2010). Structure and dynamics of the Columbia River tidal plume front. *Journal of Geophysical Research: Oceans*, *115*(5). https://doi.org/10.1029/2009JC006066

Kim, Y. H., & Voulgaris, G. (2005). Effect of channel bifurcation on residual estuarine circulation: Winyah Bay, South Carolina. *Estuarine, Coastal and Shelf Science*, *65*(4), 671–686. https://doi.org/10.1016/j.ecss.2005.07.004

Lam, P., & Kuypers, M. M. M. (2011). Microbial nitrogen cycling processes in oxygen minimum zones. *Annual Review of Marine Science*, *3*, 317–345. https://doi.org/10.1146/annurev-marine-120709-142814

Li, S., Zhang, Z., Zhou, M., Wang, C., Wu, H., & Zhong, Y. (2022). The Role of Fronts in Horizontal Transports of the Changjiang River Plume in Summer and the Implications for Phytoplankton Blooms. *Journal of Geophysical Research: Oceans*, *127*(8). https://doi.org/10.1029/2022JC018541

Lohrenz, S. E., Fahnenstiel, G. L., Redalje, D. G., Lang, G. A., Dagg, M. J., Whitledge, T. E., & Dortch, Q. (1999). Nutrients, irradiance, and mixing as factors regulating primary production in coastal waters impacted by the Mississippi River plume. In *Continental Shelf Research* (Vol. 19).

Murphy, J., & Riley, J. P. (1962). A Modified Single Solution Method for the Determination of Phosphate in Natural Water. *Elsevier*, *27*, 31–36.

Paytan, A., & McLaughlin, K. (2007). The oceanic phosphorus cycle. *Chemical Reviews*, *107*(2), 563–576. https://doi.org/10.1021/cr0503613

Schnetger, B., & Lehners, C. (2014). Determination of nitrate plus nitrite in small volume marine water samples using vanadium(III)chloride as a reduction agent. *Marine Chemistry*, *160*, 91–98. https://doi.org/10.1016/j.marchem.2014.01.010

Seitzinger, S. P., Mayorga, E., Bouwman, A. F., Kroeze, C., Beusen, A. H. W., Billen, G., Van Drecht, G., Dumont, E., Fekete, B. M., Garnier, J., & Harrison, J. A. (2010). Global river nutrient export: A scenario analysis of past and future trends. *Global Biogeochemical Cycles*, *24*(2). https://doi.org/10.1029/2009GB003587

Seitzinger, S. P., & Phillips, L. (2017). Nitrogen stewardship in the Anthropocene. In *Science* (Vol. 357, Issue 6349, pp. 350–351). American Association for the Advancement of Science. https://doi.org/10.1126/science.aao0812

Sharples, J., Middelburg, J. J., Fennel, K., & Jickells, T. D. (2017). What proportion of riverine nutrients reaches the open ocean? *Global Biogeochemical Cycles*, *31*(1), 39–58. https://doi.org/10.1002/2016GB005483

Tong, Z., Ma, L., Cai, S., Wang, L., Xiao, W., Huang, B., & Laws, E. A. (2023). Responses of Phytoplankton Communities to the Effect of Both River Plume and Coastal Upwelling. *Journal of Geophysical Research: Biogeosciences*, *128*(11). https://doi.org/10.1029/2023JG007486

Trenberth, K. E., Smith, L., Qian, T., Dai, A., & Fasullo, J. (2007). Estimates of the global water budget and its annual cycle using observational and model Data. In *Journal of Hydrometeorology* (Vol. 8, Issue 4, pp. 758–769). https://doi.org/10.1175/JHM600.1

USGS. (2024). *Water Data* . https://waterdata.usgs.gov/monitoring-location/02131000

Voss, M., Bange, H. W., Dippner, J. W., Middelburg, J. J., Montoya, J. P., & Ward, B. (2013). The marine nitrogen cycle: Recent discoveries, uncertaintiesand the potential relevance of climate change. *Philosophical Transactions of the Royal Society B: Biological Sciences*, *368*(1621).

https://doi.org/10.1098/rstb.2013.0121

Yankovsky, A. E., Fribance, D. B., Cahl, D., & Voulgaris, G. (2022). Offshore Spreading of a Supercritical Plume Under Upwelling Wind Forcing: A Case Study of the Winyah Bay Outflow. *Frontiers in Marine Science*, *8*. https://doi.org/10.3389/fmars.2021.785967

Yankovsky, A. E., & Voulgaris, G. (2019). Response of a coastal plume formed by tidally modulated estuarine outflow to light upwelling-favorable wind. *Journal of Physical Oceanography*, *49*(3), 691–703. https://doi.org/10.1175/JPO-D-18-0126.1

Zehr, J. P., & Ward, B. B. (2002). Nitrogen cycling in the ocean: New perspectives on processes and paradigms. In *Applied and Environmental Microbiology* (Vol. 68, Issue 3, pp. 1015–1024). American Society for Microbiology. https://doi.org/10.1128/AEM.68.3.1015-1024.2002